Combining Operando X-ray Experiments and Modelling to Understand the Heterogeneous Lithiation of Graphite Electrodes

SUPPLEMENTARY INFORMATION

Contents

1. Formation of the electrode (first cycle)

The electrode was prepared and cycled just before the beamtime, as shown in Figure S1. The sequence applied was:

1. lithiation for 10 h (constant current of 60 µA)
2. floating for 1 h at 5 mV
3. relaxation for about 15 min (open circuit)
4. delithiation until the cutoff potential of 1.5 V (constant current of 60 µA for 9h17m)
5. floating for 5 min (constant potential of 1.5 V)
6. relaxation for about 15 min
7. second lithiation for about 8h (constant current of 75 µA)
8. floating for 2h45 at 5 mV
9. relaxation for 30 min
10. open circuit during transfer to the beamline

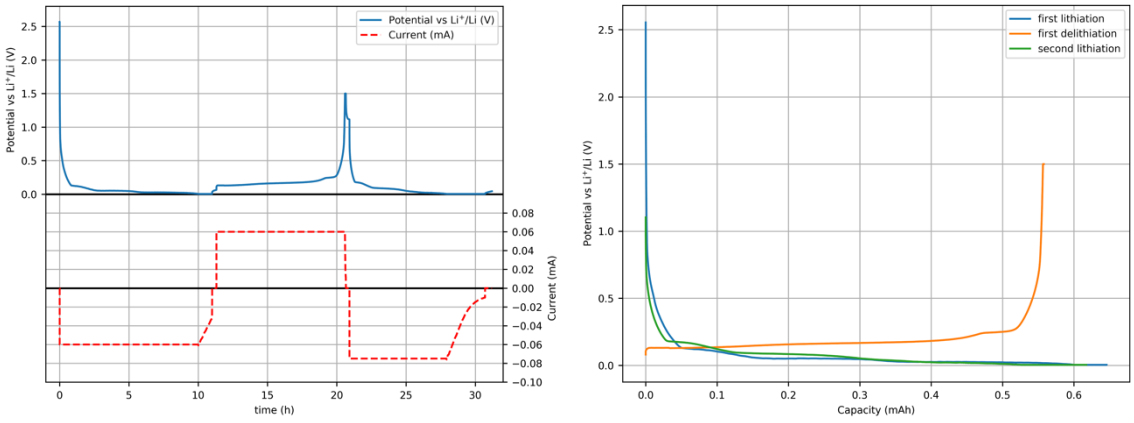

Figure S1. Potential of the operando during the preliminary cycling of the electrode, prior to the experiment, (left) as a function of time, (right) as a function of capacity.

2. Quantification of the Li content from X-ray diffraction

As described in the text, we tested different fit function to establish a relation between the average Li content x and the average q value, or correspondingly d-spacing ($d = \frac{2\pi}{q}$), of the diffraction from adjacent graphene sheets. We first found the best fit for a piecewise linear function going through the [q,x] points listed below, ordered by increasing x (and d) :

[q_0 = 1.873 Å^{-1}, x_0 = 0], [q_1, x_1], [q_2, x_2], [q_3, x_3 = 0.25], [q_4, x_4 = 0.5], [q_5 = 1.701 Å^{-1}, x_5 = 1],

solving for q_1, q_2, q_3, q_4, x_1, and x_2, with the condition that $q_1 > q_2 > q_3 > q_4$ and $x_1 < x_2$.

The extreme q, x values (q_0, x_0 and q_5, x_5) are given by our experiment: the peak from LiC_6 (x_5 = 1) is well separated from the other possible contributions and the q value is unambiguous, and the q value for the peak from graphite (x_0 = 0) is the asymptotic position at the end of delithiation. This value may possibly be affected by some graphite that would somehow have remained partially lithiated but from the intensity map in the main text, the error is clearly limited. Note that both q_0 and q_5 values fall well within reported values for the same compounds. We fixed x_4 = 0.5, where a strong change of slope can be observed in the data from the literature. No clear change of slope could be observed around x = 0.33 (LiC_{18}), so we fixed the next value x_3 to 0.25 (LiC_{24}).

The positions of the points for the best f fit function are reported in Table S1 (fixed values are in italic). From these values, we tested other f^* functions at +/- 0.004 Å (in d-spacing) and +/- 0.02 (in x value). The geometric distance between these new f^* functions and the data from the literature was computed. All f^* within twice the minimum geometric distance were kept (Figure S2), and *in fine* used to estimate the NAAD uncertainty in Figure 7 in the main text.

Point	*d* (Å)	*q* (Å^{-1})	*x*
0	*3.354*	*1.873*	*0.000*
1	3.431	1.831	0.066
2	3.491	1.800	0.250
3	3.518	1.786	0.250
4	3.521	1.785	*0.500*
5	*3.693*	*1.701*	*1.000*

Table S1. Position of the (q,x) points defining the piecewise function f used in the text. Values in italic were held for the fit.

The structure factor correction was as follows. For a given *f** function, we calculated for each *q*-value the corresponding *x* value using *f**. Then we estimated the structure factor F considering a 180° phase shift between the graphene sheets and the Li plane, using the atomic scattering factors from the International Tables of Crystallography, interpolated over the *q* range of interest. The volume correction was simply estimated supposing a linear increase of the volume V with *x*. The experimental intensity was then divided by $|F^2|/V^2$.

Using the corrected intensity, we calculated the center of mass (intensity-weighted average *q* value) at each measurement location, and thus estimated the local average *x* using *f**. The profile of *x*(*z*) could then be obtained and used to calculate the NAAD using equation 1 from the main text.

All the NAAD profiles using the different *f** functions were calculated, and the mean NAAD is plotted in Figure 9 in the main text. The shaded area corresponds to +/- 1 standard deviation across all the *f** functions used and provides an estimate of the uncertainty.

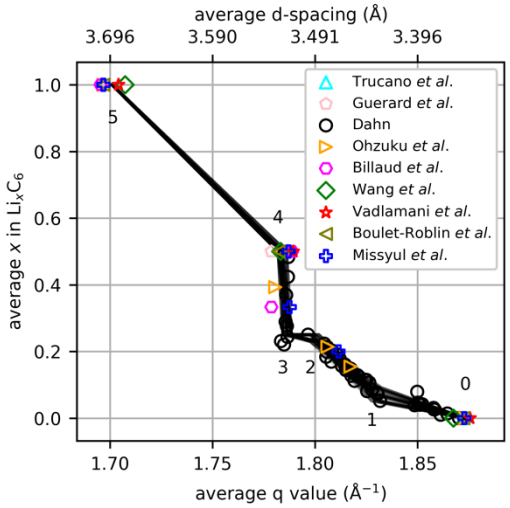

Figure S2. Different x=f(q) relations tested to estimate the robustness of the NAAD calculation and corresponding errors. Symbols are taken from the literature. References are available in the article. The solid line is least-square fit with a piecewise linear function.

3. Comparaison of the Lithium content: XRD *vs* Electrochemistry

In order to assess the quality of the XRD quantification discussed above, we compared the mean value of *x* over the whole electrode (*i.e.* the state of charge) as calculated from the XRD, and as measured with the galvanostat. The results are shown in figure S3. Differences are within ±0.1 and maybe explained by the fact that XRD is only sensitive to the ordered intercalation compounds, and that the electrochemical capacity measurements can also include electric current from other side reactions, such as SEI formation.

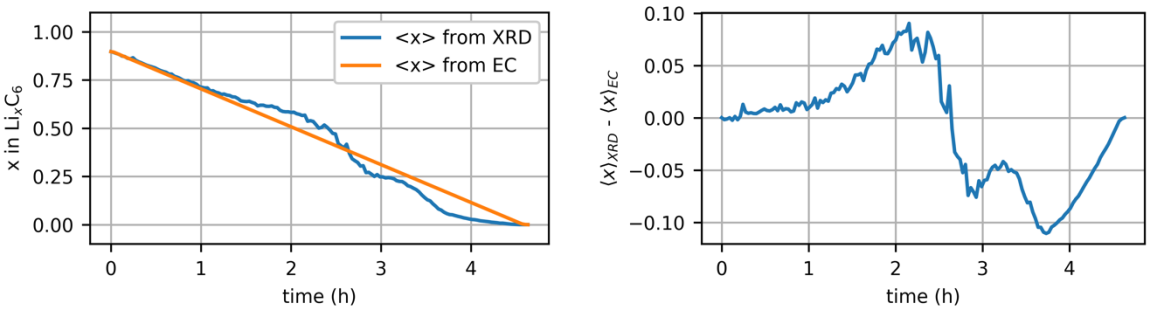

Figure S3: (left) Comparison of the Li content estimated from the XRD and electrochemical capacity (EC) measurements; (right) difference between the lithium content x measured using the microscopic XRD and the macroscopic electrochemistry as a function of the x (from the XRD).

4. Experimental reproducibility

We were able to test the reproducibility of our observation in two other instances. Firstly, we lithiated again the same sample (Sample1_Li2 in Figure S4), and secondly, we performed the initial lithiation in another similar sample (Sample2_Li1 in Figure S4). In both cases we observed the particular succession of homogeneous and heterogeneous distribution of Li content across the electrode depth, as shown by the local increases in NAAD in figure S4. Note that contrary to the case exposed in the main text (*i.e.* delithiation, *x* starting near 1 and decreasing with time), these additional measurements were performed in lithiation (*x* starting near 0 and increasing with time). Due to time constraints, in both cases we could not reach the higher stoichiometries.

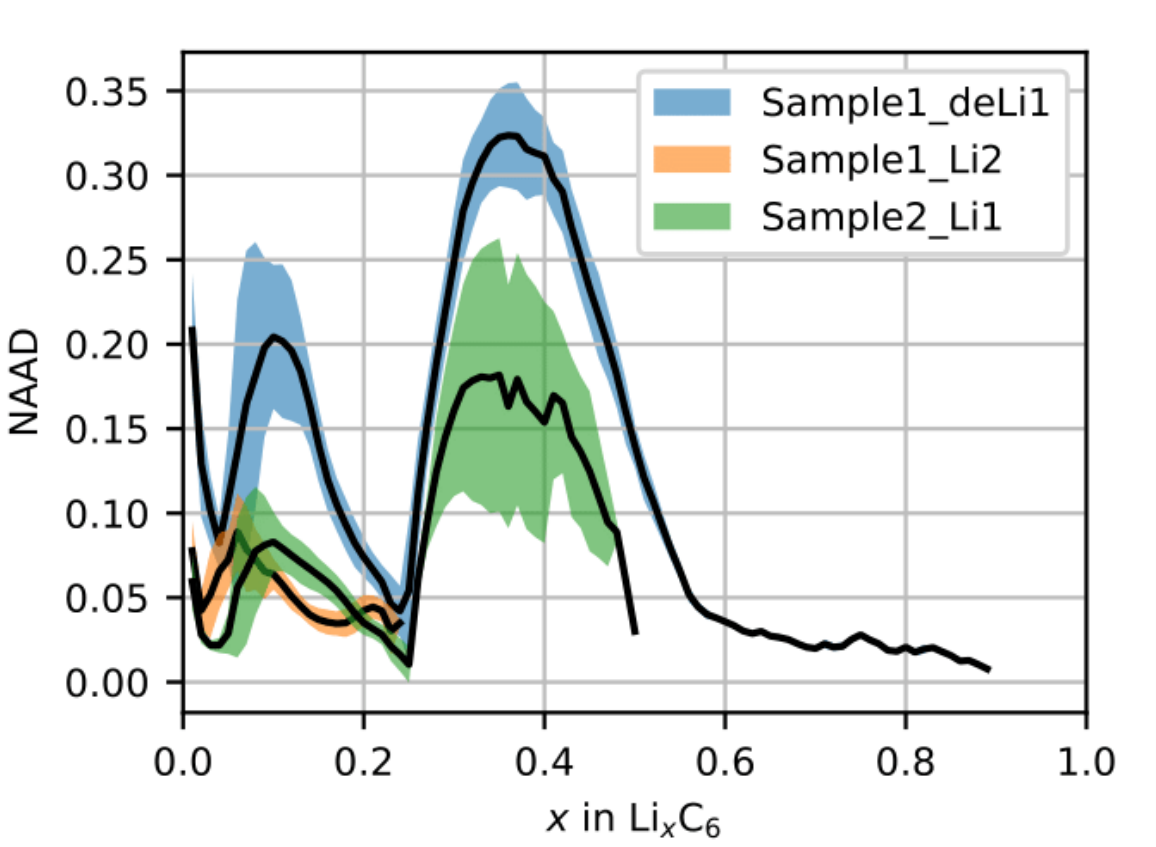

Figure S4: Comparison of the NAAD as function of the lithium stoichiometry in LixC6 for different conditions: delithiation of sample 1, following delithiation of the same sample and first lithiation of a second sample.

5. Porous Electrode Model

The graphite electrode model is based on the porous electrode theory [1]. The resolved equations are classical and a summary is provided in table S2. A more detailed description of the hypothesis is available in a previous work [2]. The two simulations described in the text were performed at a C-rate of C/5.

Graphite electrode and separator domains - Liquid phase (electrolyte)		
Mass balance	$\epsilon\frac{\partial C_l}{\partial t} - \nabla\cdot\left(D_l^{eff}\nabla C_l\right) = \frac{j_l}{F}(1-{t_0}^+)$	
Charge balance	$\nabla\cdot\left(-\sigma_l^{eff}\left(\nabla\phi_l - \frac{2RT}{F}(1-{t_0}^+)(1+\frac{dlnf^{\mp}}{dlnc})\frac{\nabla C_l}{C_l}\right)\right) = j_l$	
Currents for electrode and separator	In the graphite electrode $j_l = -j_s$	In the separator $j_l = 0$
Graphite electrode domain - Solid phase.		
Charge balance	$\nabla\cdot(-{\sigma_s}^{eff}\nabla\phi_s) = j_s$	
Currents for electrode	$j_s = a_{Gr}i_{Gr}$	
current at the active materials and electrolyte interface (Notation: $i_n = -i_{Gr}$)		
Current density at the active material/electrolyte interface	$i_n = i_o\left(exp\left(\frac{\alpha\eta F}{RT}\right) - exp\left(-\frac{(1-\alpha)\eta F}{RT}\right)\right)$	
Overpotential	$\eta = \phi_s - \phi_l - E_{eq}(x_{Li}^s, T)$	
Nominal current density	$i_o = i_{o,ref}\,(1-x_{Li}^s)^{(1-\alpha)}(x_{Li}^s)^{(\alpha)}\left(\frac{C_l}{C_{l,ref}}\right)^{\alpha}$	
active particles domains		
Mass balance	$\frac{\partial C_s}{\partial t} - \nabla\cdot(D_s\nabla C_s) = 0$	

Table S2: Governing equations of the graphite porous electrode model.

The effective properties in the porous graphite electrode and separator are computed from the porosity ϵ and tortuosity τ values for each domain: $D_l^{eff} = D_l\epsilon/\tau$ and $\sigma_l^{eff} = \sigma_l\epsilon/\tau$.

The physical parameters used in the simulations are presented in the tables below, components by components.

Parameter	**Symbol**	**Value**	**Note**
Derivation of the activity coefficient	$\frac{dlnf^{\mp}}{dlnc}$	0	Hypothesis
Transference number	t_0^+	0,363	From ref [3]
Concentration $LiPF_6$	$C_{l,ref}$	1 mol/L	From ref [2]
Lithium diffusivity	D_l	5.10^{-11} m²/s	From ref [2]
Ionic conductivity	$\sigma_l(C_l)$	$1.73 + 17.92C_l + 13.98C_l^2 + 2.67\ C_l\ ^3$	From ref [4]

Table S3: Electrolyte properties used in the model

Parameter	**Symbol**	**Value**	**Note**
Separator porosity	ϵ	0.41	From ref [2]
Separator tortuosity	τ	2.67	From ref [2]
Separator thickness	L	50µm	From ref [2]

Table S4: Separator properties used in the model

Parameter	**Symbol**	**Value**	**Note**
Composition	96 %wt Graphite / 4%wt Binder;		
Graphite weight fraction	W_{Gr}	0.96	From composition
electrode porosity	ϵ	0.35	From ref [2]
electrode tortuosity	τ	4	From ref [2]
electrode thickness	L	84.2µm	From ref [2]
electrode effective conductivity	$\sigma_s{}^{eff}$	100S/m	From ref [4] and [2]
Electrode density	ρ	2236kg/m^3	From ref [2]

Table S5: Graphite electrode properties used in the model

Parameter	Symbol	Value	Note
Mean particle radius	R_{Gr}	8µm	From ref [2]
Graphite density	ρ_{Gr}	2260kg/m^3	From ref [2]
Reversible capacity	q_{Gr}	355mAh/g	From ref [2]
Maximum lithium concentration	$C_{s,max}^{Gr}$	31 370 mol/m^3	computed
Equilibrium potential	E_e	See figure 7b,c in main text	From ref [2]
Diffusion coefficient of lithium in graphite	D_s	5.10^{-13} m²/s	From ref [4]
Symmetry coefficient for BV relation	α	0.5	Hypothesis, also ref[2]
Nominal exchange current density	$i_{o,ref}^{Gr}$	16.3 A/m²	Adjusted
Nominal exchange current density during the transition from stage 1 to stage 2 in the modified expression (See text)	$i_{o,ref}^{Gr}$	0.4 A/m²	Adjusted

Table S6: Graphite properties used in the model

In numerical models, the NAAD (see text) can be computed either for the lithium concentration at the surface of the active particles or for the mean lithium concentration inside the particles, as both quantities can be accessed. In Dufour *et al.*, the NAAD was computed for the lithium concentration at the surface of the graphite particles, as the focus was on the mechanisms at the origin of the different resistances inside the electrode [2]. The occurrence of successive heterogeneous and homogeneous distribution during the lithiation of the graphite electrode was predicuted. Using the same model, we show here that similar NAAD patterns are obtained for lithium concentration at the surface of the particles and inside the particles (figure S5), as long as the diffusion inside the graphite particles is not the limiting factor.

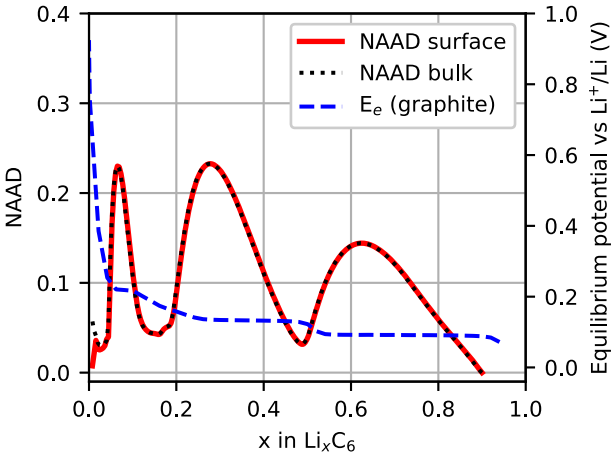

Figure S5: Comparison of the simulated NAAD of the graphite particle Li content, at the surface (thick red line) and in the bulk (black dotted line) as function of *x* in Li_xC_6 during a delithiation at C/5, and corresponding equilibrium potential of graphite (E_e, blue dashed line).

The cell voltage of the simulation with the modified exchange current density law is presented in figure S6.

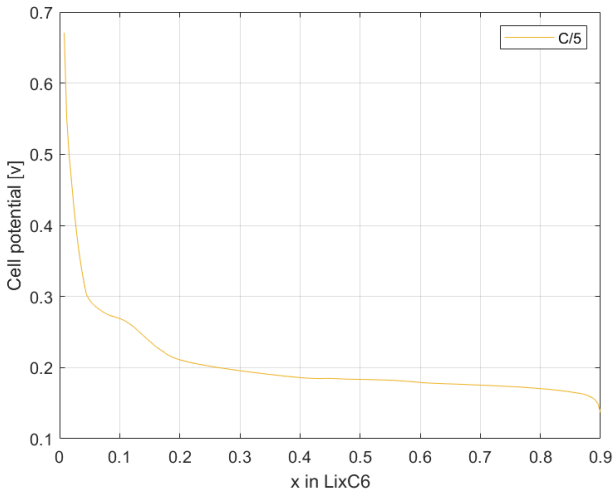

Figure S6: Simulated cell voltage during the delithiation at C/5 with the modified exchange current density law

6. References

[1] J. Newman and W. Tiedemann, Porous-electrode theory with battery applications, *AIChE J.,* 21, 25-41, **1975**

[2] N. Dufour, M. Chandesris, S. Geniès, M. Cugnet et Y. Bultel, Lithiation heterogeneities of graphite according to C-rate and mass-loading: A model study, *Electrochimica Acta,* vol. 272, pp. 97-107, **2018**.

[3] L. O. Valoen and J. N. Reimers, Transport Properties of LiPF6-Based Li-Ion Battery Electrolytes, *Journal of The Electrochemical Society,* vol. 152, pp. A882-A891, **2005**.

[4] M. Ecker, T. K. D. Tran, P. Dechent, S. Käbitz, A. Warnecke et D. U. Sauer, Parameterization of a physico-chemical model of a lithium-ion battery i. determination of parameters, *Journal of the Electrochemical Society,* vol. 162, pp. A1836--A1848, **2015**.